Ultrasound in Med. & Biol., Vol. 47, No. 9, pp. 2608–2621, 2021

0301-5629/$ - see front matter

https://doi.org/10.1016/j.ultrasmedbio.2021.05.002

● *Original Contribution*

ULTRASTRUCTURAL ANALYSIS OF VOLUMETRIC HISTOTRIPSY BIO-EFFECTS IN LARGE HUMAN HEMATOMAS

Ekaterina M. Ponomarchuk,* Pavel B. Rosnitskiy,* Tatiana D. Khokhlova,† Sergey V. Buravkov,‡ Sergey A. Tsysar,* Maria M. Karzova,* Kseniya D. Tumanova,* Anna V. Kunturova,* Y.-N. Wang,§ Oleg A. Sapozhnikov,*,§ Pavel E. Trakhtman,¶ Nicolay N. Starostin,¶ and Vera A. Khokhlova*,§

* Laboratory for Industrial and Medical Ultrasound, Physics Faculty, M. V. Lomonosov Moscow State University, Moscow, Russian Federation; † Department of Medicine, University of Washington, Seattle, Washington, USA; ‡ Faculty of Fundamental Medicine, M. V. Lomonosov Moscow State University, Moscow, Russian Federation; § Center for Industrial and Medical Ultrasound, Applied Physics Laboratory, University of Washington, Seattle, Washington, USA; and ¶ National Medical Research Center for Pediatric Hematology, Oncology and Immunology, Moscow, Russian Federation

(*Received* 24 *December* 2020; *revised* 28 *April* 2021; *in final form* 2 *May* 2021)

Abstract—Large-volume soft tissue hematomas are a serious clinical problem, which, if untreated, can have severe consequences. Current treatments are associated with significant pain and discomfort. It has been reported that in an *in vitro* bovine hematoma model, pulsed high-intensity focused ultrasound (HIFU) ablation, termed *histotripsy*, can be used to rapidly and non-invasively liquefy the hematoma through localized bubble activity, enabling fine-needle aspiration. The goals of this study were to evaluate the efficiency and speed of volumetric histotripsy liquefaction using a large *in vitro* human hematoma model. Large human hematoma phantoms (85 cc) were formed by recalcifying blood anticoagulated with citrate phosphate dextrose/saline–adenine–glucose–mannitol solution. Typical boiling histotripsy pulses (10 or 2 ms) or hybrid histotripsy pulses using higher-amplitude and shorter pulses (0.4 ms) were delivered at 1% duty cycle while continuously translating the HIFU focus location. Histotripsy exposures were performed under ultrasound guidance with a 1.5-MHz transducer (8-cm aperture, $F\# = 0.75$). The volume of liquefied lesions was determined by ultrasound imaging and gross inspection. Untreated hematoma samples and samples of the liquefied lesions aspirated using a fine needle were analyzed cytologically and ultrastructurally with scanning electron microscopy. All exposures resulted in uniform liquid-filled voids with sharp edges; liquefaction speed was higher for exposures with shorter pulses and higher shock amplitudes at the focus (up to 0.32, 0.68 and 2.62 mL/min for 10-, 2- and 0.4-ms pulses, respectively). Cytological and ultrastructural observations revealed completely homogenized blood cells and fibrin fragments in the lysate. Most of the fibrin fragments were less than 20 μm in length, but a number of fragments were up to 150 μm. The lysate with residual debris of that size would potentially be amenable to fine-needle aspiration without risk for needle clogging in clinical implementation. (E-mail: ponomarchuk.em14@physics.msu.ru)

Key Words: **High-intensity focused ultrasound, Shock waves, Boiling histotripsy, Hematoma, Compartment syndrome, Trauma, Thrombolysis, Fine-needle aspiration, Scanning electron microscopy.**

INTRODUCTION

Intra-abdominal, retroperitoneal and intramuscular hematomas are a serious clinical problem that can occur as a result of trauma, surgical intervention, bleeding disorders, blood cancer and use of anticoagulant medications and blood thinners (Elhammady et al. 2011; Dohan et al. 2015; Chung 2016; Bovonratwet et al. 2019). Large hematomas can reach liters in volume and, depending on location in the body, can cause significant pressure on the surrounding tissues leading to serious complications, including organ failure, infection, loss of limb functionality and amputation (Broderick et al. 1993; Garner et al. 2014; Chung 2016). Currently, there are no effective treatments for the immediate resolution of large hematomas. Standard of care includes drainage and surgical removal. The former is ineffective for acute clots because of their gelatinous nature, and the latter is associated with a high risk of recurrence, infection and mortality (Weiss et al. 2015; Li et al. 2020).

Address correspondence to: Ekaterina M. Ponomarchuk, Leninskie Gory, 1-2 Moscow, Russian Federation, 119991. E-mail: ponomarchuk.em14@physics.msu.ru

An alternative conservative treatment involves the gradual resolution of the hematoma over a long period, which is inapplicable in some cases because of rapidly emerging complications and pain (Smith et al. 2006). Moreover, certain types of hematomas tend to grow in size rather than resorb (Angster and Da Costa 2018).

Histotripsy, a technique using non-linear propagation of high-intensity focused ultrasound (HIFU) pulses and shock formation at the focus, was recently proposed as a rapid and minimally invasive hematoma treatment under either ultrasound or magnetic resonance (MR) guidance (Khokhlova et al. 2016a; Gerhardson et al. 2017; Ponomarchuk et al. 2019; Li et al. 2020). There are two main types of histotripsy: cavitation cloud histotripsy (CH) (Parsons et al. 2006) and boiling histotripsy (BH) (Khokhlova et al. 2015). CH uses a sequence of microsecond-long HIFU pulses with high peak negative focal pressure that generates bubble clouds at the focus; their activity mechanically homogenizes tissue (Parsons et al. 2006; Lin et al. 2014b). BH uses longer (millisecond-long) pulses with lower focal pressures that initiate highly localized boiling within each pulse as a result of tissue heating by shock fronts that develop in the acoustic waveform at the focus because of non-linear propagation effects (Khokhlova et al. 2011). Interaction between the remaining incoming shocks of the BH pulse and the expanding millimeter-sized vapor cavity results in tissue liquefaction (Khokhlova et al. 2011; Simon et al. 2012; Pahk et al. 2019, 2021). Both histotripsy approaches create purely mechanical lesions in biological tissue with negligible thermal damage when a low duty cycle (DC) of about 1% is used. The efficacy of histotripsy for liquefaction of coagulated blood has been determined *in vitro* for both vascular clots (Zhang et al. 2016) and large-volume hematomas (Khokhlova et al. 2016a; Gerhardson et al. 2017; Li et al. 2020).

Single lesions produced by BH and CH in large hematomas with the same ultrasound frequency and treatment time differ in shape and size. Single lesions produced by BH typically are "tadpole"-shaped, having a wider, round proximal region ("head") and a narrow distal region ("tail") that merge at the HIFU focus. The mechanisms responsible for such shape are still under discussion. Some studies suggest the incoming shock waves generate microfountains at the pressure release surface of the boiling bubbles, thus creating the "head" of the lesion through acoustic atomization of the prefocal tissue. The "tail" of the lesion is then generated by mechanical "chiseling" of tissue by acoustic streaming of the debris ejected by the microfountains (Simon et al. 2012). Other studies suggest an additional mechanism for lesion formation: the lesion growth starts with the formation of the "tail" containing boiling bubbles, which act as a pressure release surface for the incident waves, resulting in the generation of cavitation clouds proximal to the focus and, thus, producing the "head" of the lesion (Pahk et al. 2019, 2021). Both proposed mechanisms are likely to be involved in BH-induced tissue liquefaction, subsurface cavitation being an important part of the atomization process and relative contributions of streaming and boiling bubble expansion to the "tail" formation depending on tissue mechanical properties. The relative roles of these mechanisms may also be heavily dependent on the HIFU frequency, even within a relatively narrow range of 1−2 MHz (Khokhlova et al. 2017).

The lesion volume is contained mainly in the lesion's "head," and the focus scanning strategies in volumetric BH ablations usually aim to merge the "heads" of individual lesions, leaving the "tails" separate. BH-Induced voids are larger in volume than those created by delivering CH pulses, which are more ellipsoidal (Khokhlova et al. 2016a). Recently, a "hybrid" histotripsy approach that uses sub-millisecond pulses (intermediate between BH and CH) was proposed and successfully tested in *ex vivo* porcine liver, kidney and cardiac muscle (Eranki et al. 2018). The mechanisms involved in this approach are currently not fully understood. One hypothesis is that the use of HIFU pulses longer than CH pulses heats the tissue, reducing the cavitation threshold leading to the initiation of cavitation cloud activity (Maxwell et al., 2013; Vlaisavljevich et al., 2016). Simultaneously, tissue heating at the focus accumulates and may initiate boiling after several pulses. Thus, both mechanisms may be involved in this hybrid approach. Single lesions generated by hybrid histotripsy are similar in shape to but larger than the CH lesions and smaller than the BH lesions.

Volumetric histotripsy lesions are typically produced by generating lesions over a discrete spatial grid with specific spacing in transverse and axial directions, allowing them to merge into a volumetric void (Gerhardson et al. 2017; Khokhlova et al. 2016a, Khokhlova et al., 2019; Li et al. 2020). It has been reported that using tighter spacing with fewer pulses per sonication point results in more rapid volumetric liquefaction (Gerhardson et al. 2017; Bawiec et al. 2021). This study aimed to improve the liquefaction rate further and potentially provide more uniform liquefaction by using continuous HIFU focus translation within the targeted volume of hematoma. A secondary goal was to compare the efficiencies of the BH and hybrid regimes and the regularity of lesion borders.

The hematoma lysate generated with histotripsy should be amenable to fine-needle drainage when considering the clinical treatment of hematomas. Thus, the residual fragments within the lysate have to be small enough not to clog the needle. In prior studies, the size distribution of the residual debris was measured with a Coulter counter (Khokhlova et al. 2016a; Li et al. 2020). However, the

upper limit of the measurement system in those studies was 70 μm, which was determined by filtering the lysate before measurement to avoid clogging the system. One way to determine the sizes of larger debris fragments is through scanning electron microscopy (SEM). SEM of blood clot samples has been used extensively in studies of fibrinolysis (Weisel and Litvinov, 2008) and the influence of the presence of red blood cells (RBCs) on clot structure (Gersh et al. 2009), thrombolysis (Janis et al. 2002; Sutton et al. 2013; Bester et al. 2018) and other ultrastructural examination of clots (Pretorius et al. 2011). Here we suggest the use of SEM analysis for sizing of post-histotripsy fragments in liquefied lysate.

The overall goal of this study was to investigate and compare the efficiency and quality of BH and hybrid histotripsy in the volumetric liquefaction of large human hematoma phantoms under continuous HIFU focus translation. The measures of efficiency included the rate of liquefaction, the structure of the lesion borders and the degree of hematoma disintegration, as evaluated by light microscopy and SEM.

METHODS

Human hematoma model

After informed consent was obtained, fresh human blood was collected from healthy volunteers through sterile venipuncture according to the guidelines and after approval of the review board of the Dmitry Rogachev National Research Center (Moscow, Russia). Citrate phosphate dextrose solution was used as an anticoagulant, and saline−adenine−glucose−mannitol solution was used to provide improved preservation of RBCs (MacoPharma S.A., Tourcoing, France). The anticoagulated whole blood (450 mL) was stored in the refrigerator (+4˚C) for 1 d. One day after blood collection, 85 mL of anticoagulated blood was poured into a rectangular plastic mold and de-gassed in a vacuum desiccator at 0.1-bar residual pressure for 1 h. After de-gassing, the blood was recalcified with $CaCl_2$ solution (DalHimFarm, Russia) to a final concentration of 25 mM at 37˚C for approximately 30 min until complete coagulation occurred (Khokhlova et al. 2020). Before the histotripsy exposure, the hematoma samples were embedded into a 6% agar gel (Kotanyi, Austria), which served as an acoustically transparent container for the samples as illustrated in Figure 1a.

Histotripsy experimental arrangement

For histotripsy exposures, the hematoma phantom in the agar gel was transferred into a plastic holder, attached to a 3-D positioning system (Precision Acoustics UMS3, Dorset, UK) and immersed in de-gassed water (Precision Acoustics Water Treatment System, Dorset, UK) (Fig. 1b, 1c). The treatment was performed 3−4 h after the start of coagulation using a custom-built 1.5-MHz 12-element spherically focused transducer with an 80-mm aperture, 60-mm focal length and 24-mm-diameter central opening ($F\# = 0.75$) powered by a custom-built amplifier (Maxwell et al. 2017). Here $F\#$ or F-number is defined as the ratio of the focal length of the source to its aperture; therefore, it is a measure of the focusing angle of the source. B-Mode ultrasound was used for targeting and sonication guidance. A linear ultrasound imaging probe (ATL L7-4 probe, 4−7 MHz, Philips, Bothell, WA, USA) was aligned with the HIFU focal plane, as illustrated in Figure 1 (b, c) and was controlled by a Verasonics V1 system (Redmond, WA, USA).

Exposure parameters

Three sets of exposure parameters (Table 1) were used to generate volumetric lesions in n = 21 hematoma

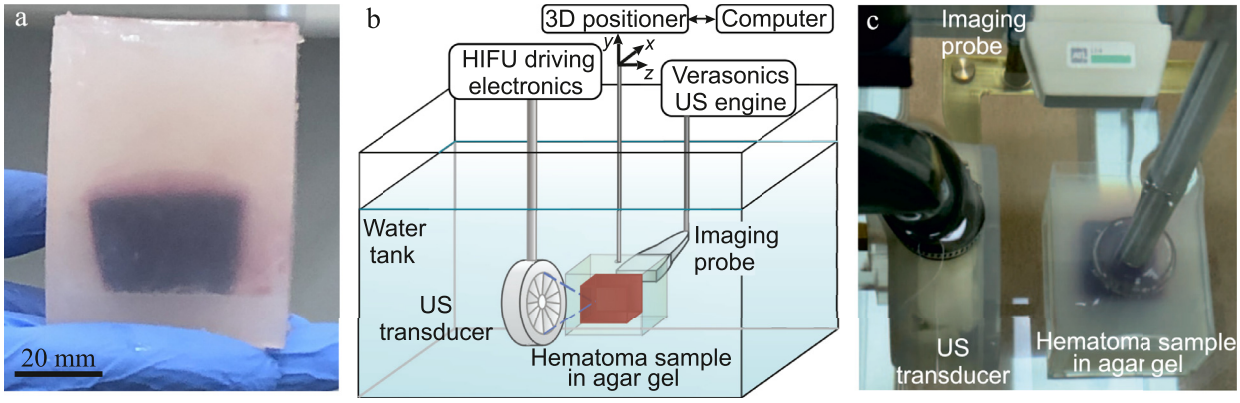

Fig. 1. (*a*) Human hematoma phantom in agar gel. (b, c) Schematic (b) and photograph (c) of the experimental setup for histotripsy liquefaction of human hematoma phantoms. B-Mode ultrasound imaging was performed with Verasonics V1 imaging system and ATL L7-4 probe. HIFU = high-intensity focused ultrasound; US = ultrasound.

Table 1. Exposure parameters for volumetric liquefaction of human hematoma phantom in boiling histotripsy and hybrid histotripsy regimes

	F#	f_0 (MHz)	t_{pulse} (ms)	N_p	Duty cycle	$W_{hematoma}$ (W)	$P^+/\lvert P^-\rvert/A_s$ (MPa)	t_b (ms)
Boiling histotripsy	0.75	1.5	10 2	8	1%	238.7	120/17/101	1.85
Hybrid			0.4	11		424	148/21/151	0.55

F# = F-number; f_0 = operational ultrasound frequency; t_{pulse} = pulse duration; N_p = equivalent number of pulses per point (N_p); $W_{hematoma}$ = acoustic power *in situ;* $P+$ ($P-$) = peak positive (negative) pressure at the focus, A_s = shock amplitude; t_b = time to boil.

samples. Two regimes used pulse durations typical for BH in soft tissues (10 and 2 ms) with a 1% DC and were applied in n = 6 samples per parameter set (Khokhlova et al. 2011). The third sonication regime others have employed for hybrid histotripsy uses sub-millisecond pulses (0.4 ms), which are noticeably shorter than BH pulses but much longer than typical CH pulses (Eranki et al. 2018), and was applied to n = 9 samples. The number of samples per BH regime was limited by the total available blood volume with citrate phosphate dextrose/saline−adenine−glucose−mannitol collected in a regular donor blood container. Because the hybrid regime was less studied, the number of samples for this treatment was increased.

For BH regimes, the necessary output power was calculated based on the required time-to-boil (t_b) *in situ,* which had to be less than the pulse duration (Khokhlova et al. 2018b). Specifically, using the combination of the heat transfer equation and weak shock theory, the required shock amplitudes *in situ* were calculated as follows (Hamilton and Blackstock 1998; Canney et al. 2010; Khokhlova et al. 2011):

$$A_s = \sqrt[3]{\frac{\Delta T c_v 6\rho^2 c_0^4}{\beta f_0 t_b}} \quad (1)$$

For the operating HIFU frequency f_0 = 1.5 MHz, the shock amplitude had to be higher than 57.5 and 98.3 MPa for time-to-boil to be less than 10 and 2 ms, respectively. The temperature difference, ΔT, in eqn (1) is the difference between the ambient temperature and 100˚C. Heat capacity per unit volume (c_v) in human blood clot was calculated as heat capacity per unit mass, previously measured by Nahirnyak et al. (2006), multiplied by the clot density ρ = 1060 kg/m^3: c_v = 3.71 MJ/m^3•K (Nahirnyak et al. 2006). The sound speed in human blood clot, c_0 = 1585 m/s, its density ρ = 1060 kg/m^3 and non-linear parameter β = 4.15 were also taken from the literature (Shung et al. 1984; Nahirnyak et al. 2006; Khokhlova et al. 2016a). In the above calculations, thermal diffusion was considered to be negligible.

Note that the same output power was used for both BH regimes (Table 1), with the theoretical time-to-boil of 1.85 ms being within both 10- and 2-ms pulse lengths. This is because a shock amplitude <100 MPa is achieved when the shock is not fully developed for the highly focused transducer used in this work. This regime is very sensitive to fluctuations in output acoustic power or inhomogeneities encountered in the acoustic path and is therefore not very reliable (Khokhlova et al. 2018b). The output power level required to achieve the necessary shock amplitude at the focus in the hematoma sample was determined based on previous acoustic characterization of this HIFU system via combined hydrophone measurements and modeling (Khokhlova et al. 2018b, 2018c, Yuldashev et al. 2018) in combination with a non-linear derating procedure (Bessonova et al. 2010; Canney et al. 2010):

$$W_{hematoma} = W_{water} e^{2\alpha D} \quad (2)$$

W is the output acoustic power in water and in the hematoma producing the same focal waveform, α = 0.076 Np/cm is the attenuation coefficient of the clotted blood at 1.5 MHz (Shung et al. 1984) and D = 11 mm is the mean depth of HIFU focus in tissue. The equivalent source parameters for modeling based on the wide-angle parabolic equation were as follows: 72.7-mm aperture, 60-mm focal length, 30-mm-diameter central opening and a scale factor p_0/V_0 = 4.508 kPa/V for conversion from the pressure at the transducer surface to the applied voltage.

For the hybrid regime, the highest achievable power of the amplifier was used. Bubble activity initiation was verified experimentally by observing a bright hyperechoic region on the B-mode image after delivering a single BH pulse or several 0.4-ms pulses.

The numerically modeled *in situ* focal waveforms corresponding to the power levels used in each regime are illustrated in Figure 2. Parameters of these waveforms are provided in Table 1. For the hybrid regime (t_b = 0.55 ms), time-to-boil was calculated to be slightly longer than the pulse duration, which corresponded to the experimental observations of the bright spot on B-mode images.

Sonication geometry

Volumetric histotripsy lesions (3−4 mL in volume) were generated by continuous translation of the transducer focus along a square-wave trajectory (Fig. 3) in

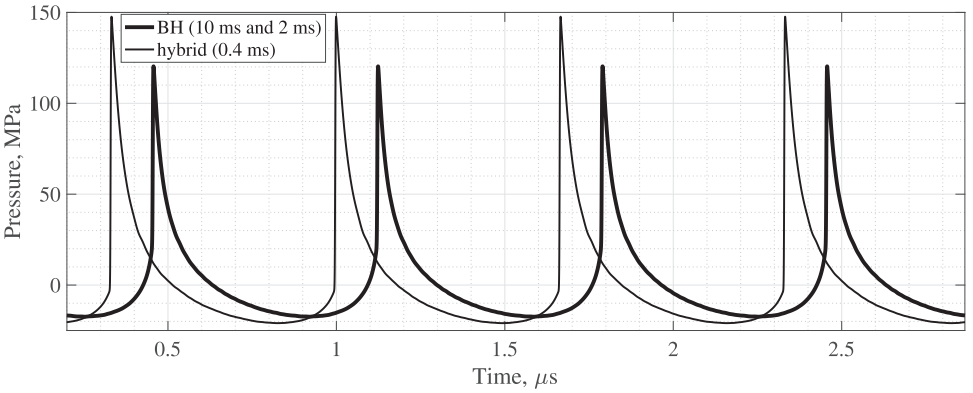

Fig. 2. Simulated waveforms for boiling histotripsy (BH) and hybrid histotripsy regimes in the hematoma phantom, at the focus of the 1.5-MHz transducer. The waveforms were calculated using a wide-angle parabolic equation with an equivalent source method combining hydrophone measurements in water with a non-linear derating procedure.

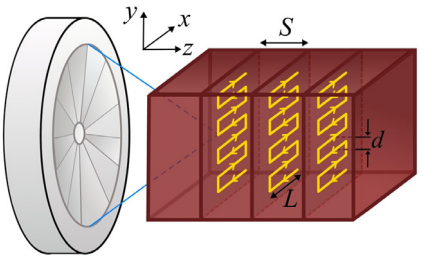

Fig. 3. Focus translation trajectory for producing volumetric lesions.

several transverse planes, starting distally and progressing proximally. The folding parameter d (*i.e.,* the distance between the lesion lines) and spacing between the layers S were determined so that the nearest lines of the lesions effectively merged to produce homogeneous volumetric lesions. The choice was based on the preliminarily measured sizes and shapes of single lesions produced with a number of pulses N_p (Table 1) from B-mode images and gross photographs (see the Results section) for each set of exposure parameters. For the BH regimes, the optimal number of pulses per point was selected as $N_p = 8$ based on the rapid increase in the void size with the number of pulses up to that number (Khokhlova et al. 2018a). The folding parameter d was chosen to be about 50% smaller than the diameter of the corresponding lesion "heads" to merge the lesions produced in adjacent lines. Focus translation speed, υ, was calculated such that an equivalent number of pulses, N_p, would be deposited per focus, assuming the same distance, d, between single foci in a line as between the lines of lesions (Fig. 3): $\upsilon = d/(t_{pulse} \bullet 100 \bullet N_p)$. For the hybrid regime, because single lesions were much smaller, the optimal equivalent number of pulses per point, $N_p = 11$, was determined by sonicating separate lines with varying focus translation speeds to produce continuous lesion lines at the fastest rate. The liquefaction rate, in cubic centimeters per minute, was estimated as the square of the line width multiplied by its length and focus translation speed.

Analysis of histotripsy outcome

Lesion size evaluation and gross analysis. The length and width of the lesions (*i.e.,* in z and x directions, see Fig. 3) were first measured based on B-mode images of the hypo-echoic area that formed about 5–10 min after the exposure. This hypo-echoic area corresponded to the liquefied part of the hematoma. After the treatment, samples were bisected first in the xy plane and then in the axial plane for gross observation and photography in all three dimensions. The width, length and depth of the lesions (*i.e.,* dimensions in x, y and z directions, see Fig. 3) were also measured from these gross photographs and compared with those measured from B-mode images. The approximate lesion volume was then calculated as a product of the three measured dimensions.

Sample collection. After the treatment, two samples for each of the three treatment regimens were randomly selected for cytological and ultrastructural analysis. After the samples were bisected, the liquefied content was aspirated from the lesions using an 18G needle for subsequent light microscopy and SEM.

Small fragments of intact hematoma captured from its volume with an 18G fine needle immediately after recalcification and 3 h later served as control untreated samples for both cytology and SEM.

Light microscopy. One drop of the aspirated lysate was smeared on a glass slide, fixed with May–Grunwald solution and stained using Wright–Giemsa stain. The smears were photographed at 40 × magnification on a

Zeiss Axio Imager (Oberkochen, Germany) light microscope equipped with a color digital camera (AxioCam MRc5, 2584 × 1936-pixel resolution, Zeiss).

Scanning electron microscopy. For ultrastructural analysis, a drop from each sample was placed on a 10-mm-diameter round coverglass substrate, fixed using 2.5% glutaraldehyde solution (DC Panreac, Barcelona, Spain) and dehydrated in ethanol of increasing concentration. Dehydrated samples were soaked in hexamethyldisilazane (Sigma-Aldrich, St. Louis, MO, USA) and air-dried before mounting and gold sputtering (Buravkov et al. 2011). The choice of the glass substrate over carbon adhesive tape as a substrate was made based on preliminary observations of the ultrastructure of different substrates, so that they would not be confused for the fibrin structure. The lysate samples were examined and photographed using a JEOL JSM-6380LA Analytical Scanning Electron Microscope (Tokyo, Japan).

To examine individual debris within the lysate drop, as opposed to multiple fused layers of debris, the lysate was diluted either in phosphate-buffered saline (PBS, PanEco, Kantemirovskaya, Russia) or in distilled water. The use of distilled water was expected to result in bursting of white blood cells and RBCs because of osmotic pressure. However, the structure of the fibrin network segments was expected to remain unaffected by dilution in water, and the cell sizes (6−8 μm in diameter) were significantly smaller than the largest residual fibrin fragment of interest. The samples obtained with dilution in PBS were also examined under SEM for comparison.

Before the histotripsy experiments, fresh human blood was diluted with PBS at concentrations of 1:25, 1:50, 1:75 and 1:100, placed on a glass substrate and prepared for subsequent SEM investigation. The results of these experiments provided the optimal dilution level resulting in complete separation of blood cells and no overlap of them in SEM images, with spacing sufficient for separating larger fibrin network fragments (>70 μm) expected to be observed in liquefied lysate after the treatment.

After histotripsy exposures, a part of the liquefied content from each sample of the group was diluted with either PBS solution or distilled water at a concentration of 1:50 (the optimal dilution level defined as described above) and prepared for subsequent SEM analysis. Each SEM sample, approximately 8−10 mm in diameter, was scanned in its entirety and examined for fragments noticeably larger than RBCs (above 20 μm) to eliminate RBCs from sizing and focus on large fibrin net fragments only. These fragments were photographed (overall 23 fields of view) and analyzed in ImageJ (National Institutes of Health, Bethesda, MD, USA). Each fragment was manually outlined, and the "maximum Feret diameter" was used as a measurement of fragment size.

To determine whether fine-needle aspiration influenced the ultrastructure of samples being observed on SEM, a preliminary experiment with human native blood was performed. A drop of human native blood was placed on a substrate and allowed to clot at 37°C. An 18G needle was used to aspirate part of the clotted drop. The ultrastructure of the blood clot collected by the needle was compared with that of the clot left on the substrate using SEM (Fig. 4). No apparent differences were observed. Both the structure of the fibrin network (indicated by *white arrows* in Fig. 4) and the shape of the cells (seen under low magnification, Fig. 4a, 4b) remained the same, which can be seen even under high magnification (× 12,000). These results indicate that fine-needle aspiration did not alter the ultrastructure of the aspirated material.

RESULTS

Single lesions

B-Mode images of single lesions produced by delivering N_p = 8 pulses of the BH regimes and lines of lesions obtained with N_p = 11 pulses per sonication point of the hybrid histotripsy regime are provided in Figure 5. The single lesions induced by BH have the typical "tadpole" shape (Fig. 5a, 5b). Delivery of shorter pulses resulted in axially shorter lesions (both heads and tails were shorter), with the narrower "head" being almost the same width as the "tail" (Fig. 5c). Sonication geometry parameters and focus translation speed (Table 2) were determined by the size of these lesions (Fig. 5) to achieve effective merging of BH single lesions (primarily the "heads") and lesion lines for the hybrid regime.

In-treatment ultrasound imaging and gross observations

Untreated phantoms (Fig. 6a) appeared mildly echogenic on B-mode images, in agreement with literature on the sonographic appearance of hematomas (Wicks et al. 1978). The echogenicity stems from scattering by RBCs trapped within the fibrin network. During the exposure (10 ms regime), the treated area appeared as a bright hyperechoic region because of the presence of vapor and gas bubbles (Fig. 6b). As the bubbles dissolved after the treatment, the liquefied lesion gradually turned hypo-echoic over 10 min (Fig. 6c).

B-Mode ultrasound images of volumetric lesions and gross photographs of the voids after sample bisection for each of the regimes used are provided in Figure 7. Note that the B-mode images (Fig. 7a−c) are shown in the axial plane of the HIFU transducer (*xz* plane containing the transducer acoustic axis, Fig. 2), and the gross photographs (Fig. 7d−f) are in the transverse plane (*xy* plane, perpendicular to the transducer acoustic axis, Fig. 2). Five to ten minutes after the exposures (Fig. 7a,

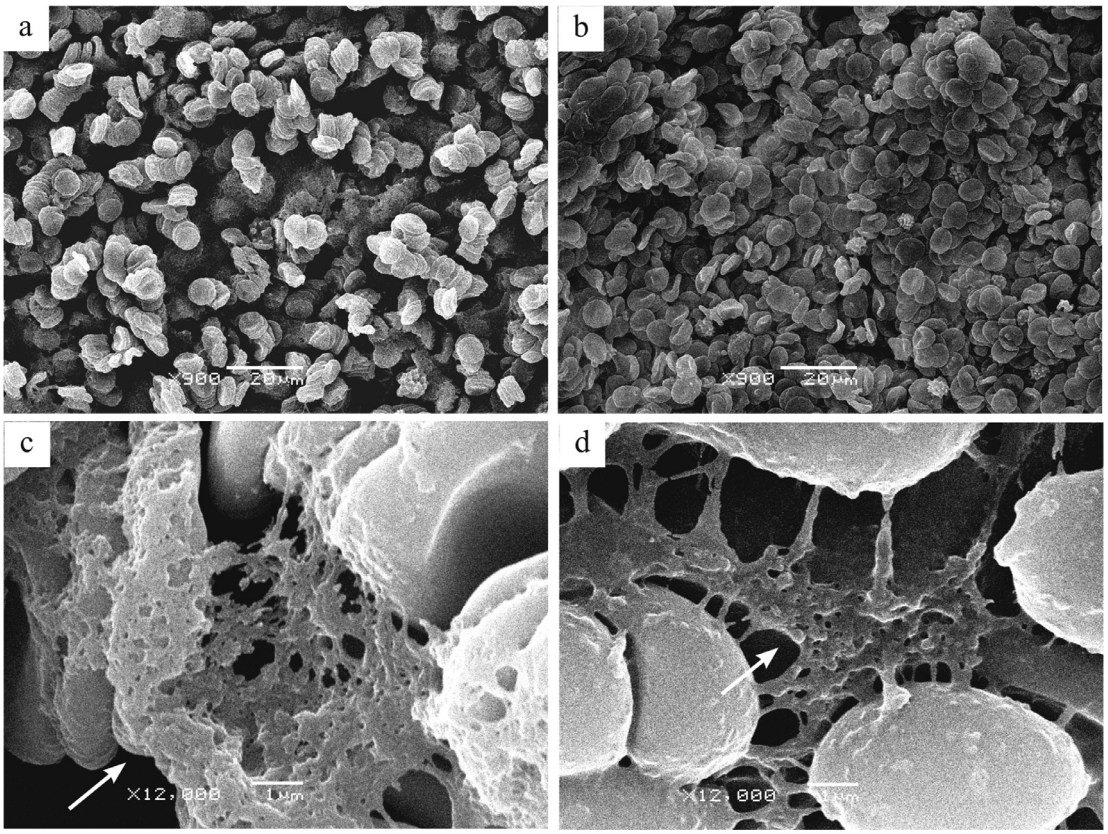

Fig. 4. Influence of fine-needle aspiration on the ultrastructure of clot components. The content of the human blood clot: (a, c) aspirated by a needle; (b, d) left on a substrate. *White arrows* point to fibrin network. Bars = (a, b) 20 μm and (c, d) 1 μm.

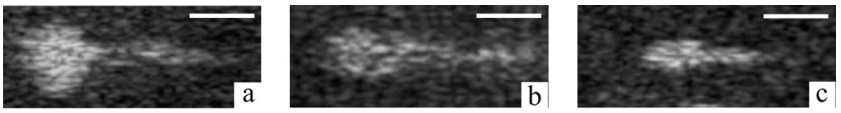

Fig. 5. B-Mode images of single lesions (high-intensity focused ultrasound incident from the left) induced by (a) eight 10-ms pulses, (b) eight 2-ms pulses and (c) eleven 0.4-ms pulses. Bars = 5 mm.

Table 2. Parameters of experimentally performed large-volume hematoma treatments in boiling histotripsy regimes and suggested hybrid histotripsy

	t_{pulse} (ms)	Focus translation speed, v (mm/s)	Maximum lesion volume (cm^3)	Treatment time (min)	Maximum liquefaction rate (mL/min)
Boiling histotripsy	10	0.45	3.34	11	0.3
	2	1.1	3.56	5.23	0.68
Hybrid	0.4	5	3.67	1.4	2.62

7b), the volumetric lesions appeared as hypo-echoic areas of completely liquefied material. The *white-dashed rectangles* in Figure 7 outline the lesions, as defined by the B-mode image taken after the bubbles dissolved. Note that the image in Figure 7c was taken before the treated area turned fully hypo-echoic to illustrate that the bubbles were pushed toward the lesion "tails" and dissolved later than those in the proximal part of the liquefied volume. The irregular "tadpole" of individual single BH lesions resulted in a volumetric homogenized proximal area and distal hypo-echoic regions of discrete "tails" (marked by *white arrows* in Fig. 7a, 7b). The volume disrupted by these discrete "tails" was not included in the overall volume estimation.

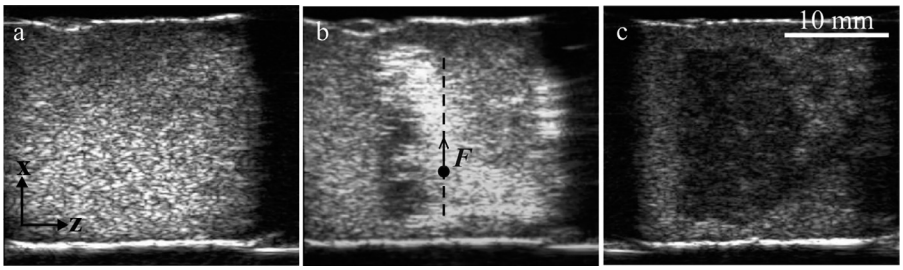

Fig. 6. B-Mode imaging of a volumetric boiling histotripsy lesion produced with 10-ms pulses (high-intensity focused ultrasound incident from the left): (a) before treatment, (b) during treatment of the distal layer with the focus (*F*) moving transversely to the transducer axis, and (c) 5 minutes after treatment. The *black dashed line* in (b) indicates the trajectory of the transducer focus movement. Bars = 10 mm.

The samples were bisected along the proximal edge of the lesion in the *xy* plane (Fig. 7d–f). Lesion volume measurements made from B-mode and gross images are outlined in Table 2. The size of the lesions along the *x*-axis agreed well with the size of those obtained from the corresponding B-mode images. No apparent differences in lesion contents between different pulsing protocols could be discerned by gross observation.

Liquefaction rate

The liquefaction rate for each of the three sonication regimes was calculated from the measured liquefied void size and sonication time (Table 2). In this study, the highest thrombolysis rate of 2.62 mL/min was achieved with sub-millisecond pulses (0.4 ms).

Cytological analysis

Regardless of the time point after blood recalcification, the control untreated hematoma samples stained with Wright–Giemsa stain appeared as densely packed RBCs and leukocytes under light microscopy (Fig. 8a). Regardless of the histotripsy exposure parameters, smears of the lesion lysate revealed non-viable shadows of erythrocytes and destroyed white blood cells with

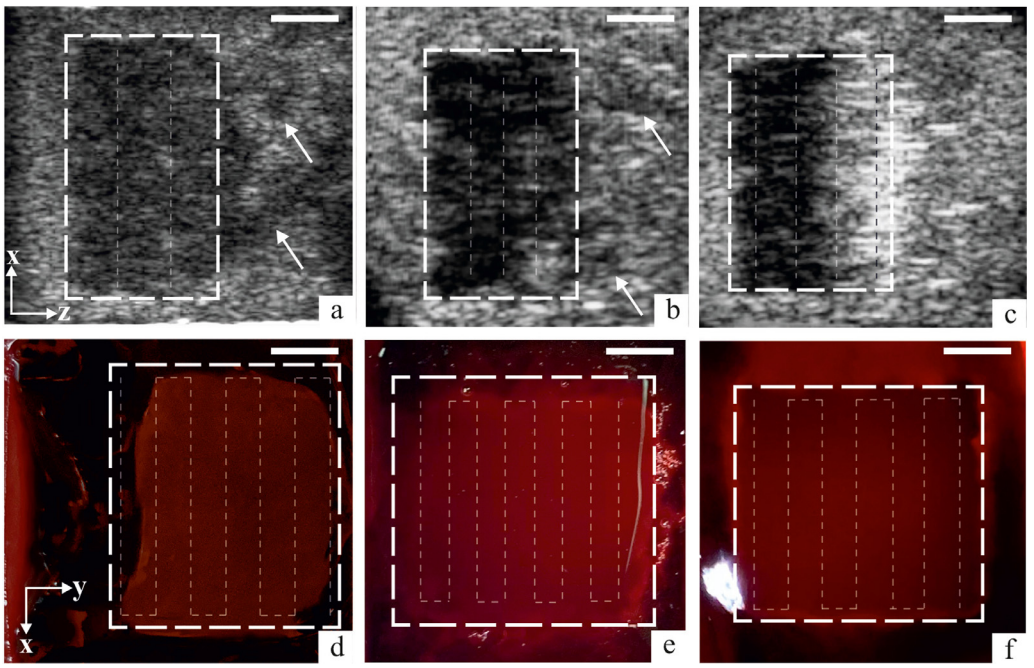

Fig. 7. (a–c) B-Mode images (HIFU incident from the left, along the *z* axis) and (d–f) bisection photos (HIFU incident perpendicularly to the image plane) of the volumetric lesions induced by BH with 10-ms pulses (left column) and 2-ms pulses (middle column) and by the hybrid regime with 0.4-ms pulses (right column). *White dashed boxes* outline the volumetric lesions. In the B-mode images (a–c), *narrow dotted lines* indicate the layers of transducer focus translation. In the bisection photos (d–f), *narrow dotted lines* indicate transducer focus translation trajectory in each layer. Bars = 5 mm.

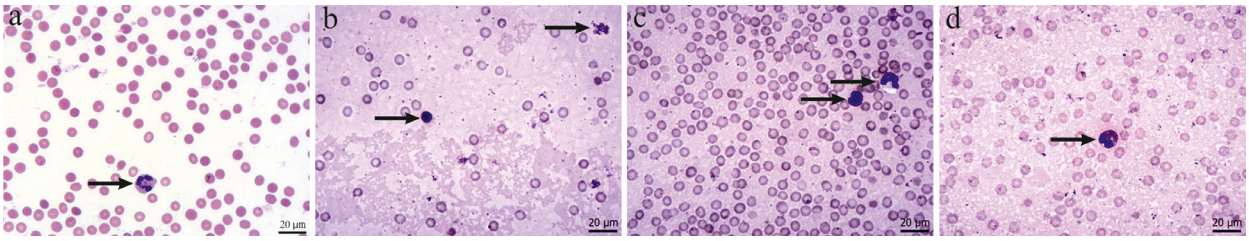

Fig. 8. Light microscopy images of (a) intact hematoma and (b–d) hematoma lysate treated with boiling histotripsy pulses of (b) 10 ms and (c) 2 ms and with the hybrid regime using 0.4-ms pulses (d). Bars = 20 μm. *Black arrows* point at leukocytes: (a) intact, (b–d) destroyed. Treatment-induced hemolysis appears as tinted background (b–d).

condensed nuclei and no cell membrane (Fig. 8b–d). The pink-tinged background seen after histotripsy exposure indicates hemolysis caused by the treatment. No influence of treatment protocol was observed on the lysate contents under light microscopy.

Scanning electron microscopy of untreated hematoma and histotripsy lysate

Two control samples of untreated hematoma were aspirated for SEM: one was taken immediately after recalcification was visually complete (Fig. 9a, 9c), and the other 3 h later (Fig. 9b, 9d). As seen in Figure 9, the ultrastructure of visually clotted blood had changed over the 3 h after recalcification; fibrin fibers between RBCs were more clearly seen at the latter time point. These changes were in agreement with the literature (Bernal et al. 2012), as the elastic properties of the large volume clot were shown to be changing over the first 3 h after the start of coagulation.

In the treated hematoma samples (Fig. 9), only multilayered fibrin network debris was visible, regardless of the treatment protocol (Fig. 10). Higher magnification revealed layered fragments of destroyed fibrin network covered with cell remnants (Fig. 10d–f).

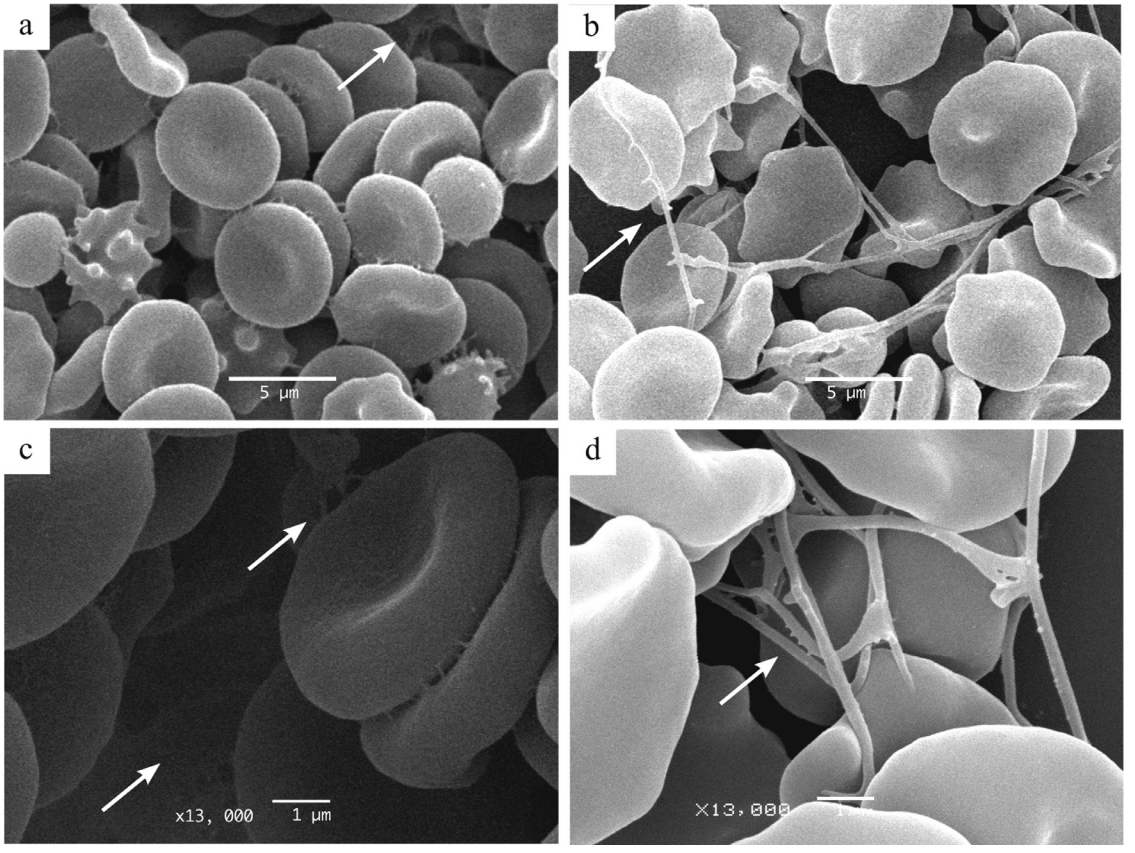

Fig. 9. Scanning electron microscopy control images of intact hematoma immediately after recalcification (a, c) and 3 h after recalcification (b, d). Bars = (a, b) 5 μm and (c, d) 1 μm. *White arrows* point at fibrin fibers.

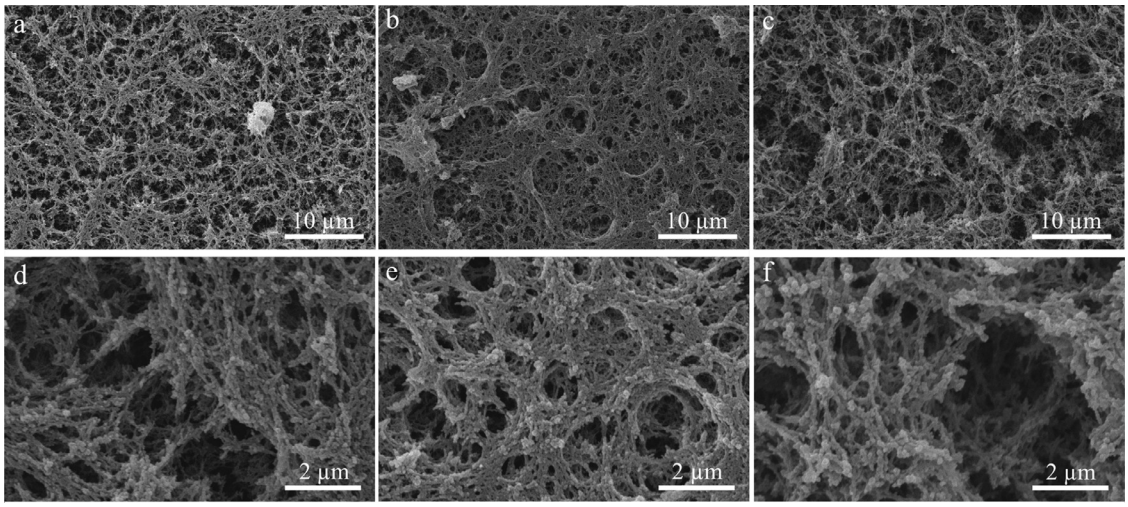

Fig. 10. Scanning electron microscopy images of hematoma lysate treated with boiling histotripsy pulses of (a, d) 10 ms and (b, e) 2 ms and with the hybrid regime using 0.4-ms pulses (c, f). Bars = (a–c) 10 μm and (d–f) 2 μm.

Scanning electron microscopy of diluted lysate

To separate the residual fibrin network debris while maintaining the isotonicity of the blood components, a group of lysate samples were diluted with PBS. As a result, individual residual clot components were more clearly observed. However, occasional salt crystals were detected, leading to adhesion of initially separated clots to those crystals and, thus, hindering the analysis of the debris (Fig. 11a, 11d).

To avoid the aggregation of clot segments with salt crystals, the lysate was diluted with distilled water. As expected, the use of distilled water led to bursting of blood cells (Fig. 11b, 11e), whereas fibrin ultrastructure present in the lysate remained the same as that observed in samples diluted with PBS, even at a magnification of × 13,000 (Fig. 11c, 11f).

Dilution of the lysate with distilled water allowed for evaluation of the size of individual fibrin network

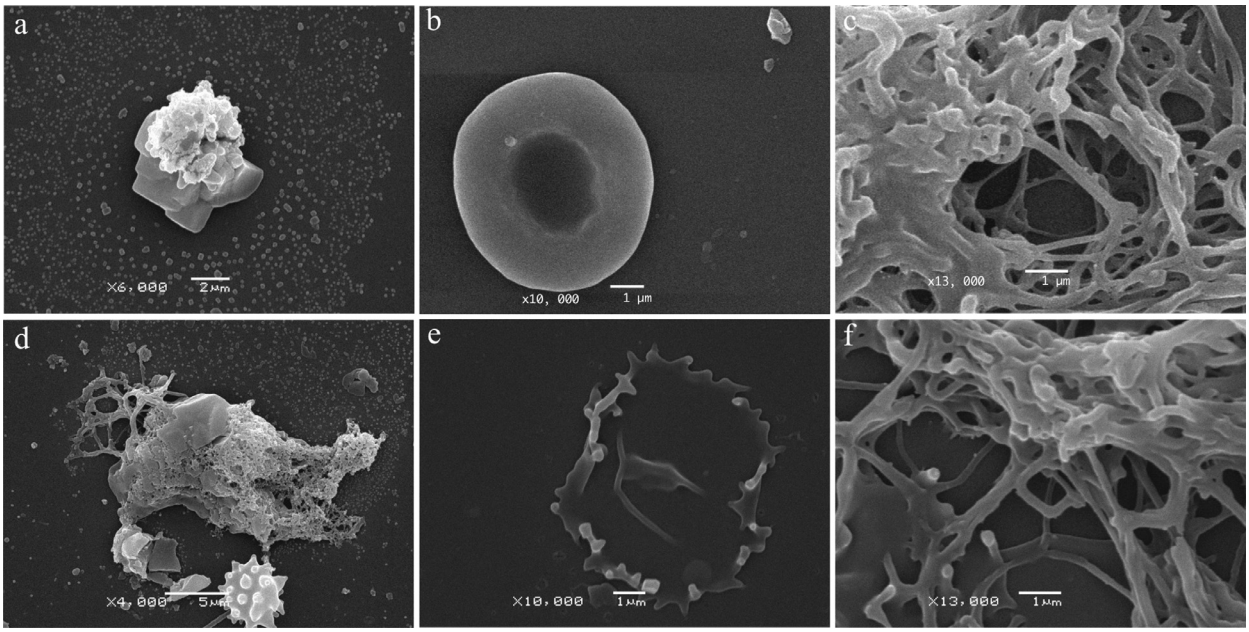

Fig. 11. Scanning electron microscopy images of (a, d) salt crystal artifacts with aggregated clot debris after dilution of the lysate in phosphate-buffered saline solution. Red blood cells (b, e) and ultrastructure of fibrin fibers (c, f) after dilution in phosphate-buffered saline solution (b, c) or in distilled water (e, f). Bars = (a) 2 μm, (b, c, e, f) 1 μm and (d) 5 μm.

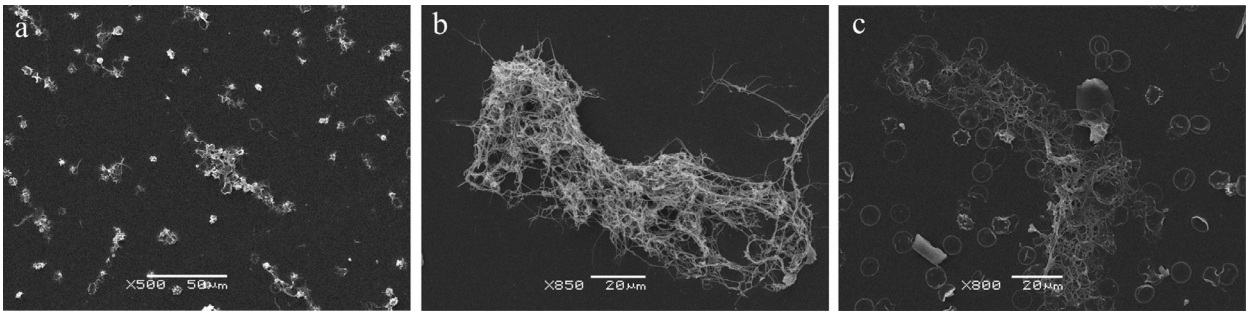

Fig. 12. (a) Gross scanning electron microscopy image of the lysate diluted with distilled water at a concentration 1:50. (b, c) Scanning electron microscopy images of the largest fibrin network fragments present in the lysate diluted with distilled water after the treatment. Bars = (a) 50 μm and (b, c) 20 μm.

Table 3. Size distribution of large fragments (>20 μm) in the diluted lysate of the test group samples

Size	No. of fragments
20−50 μm	17
50−100 μm	7
100−150 μm	4

segments (Fig. 12a). Table 3 outlines size distribution of the residual fragments larger than 20 μm. Regardless of the histotripsy treatment protocol, the largest of the fibrin segments that remained after the exposures were 150 μm in length and are illustrated in Figure 12 (b, c).

DISCUSSION

The ultimate goal of this study was to optimize histotripsy regimes for liquefaction of large-volume hematomas in terms of maximizing the thrombolysis rate while providing means for unobstructed fine-needle aspiration, as evaluated from the residual fragment sizes. We have evaluated the performance of different histotripsy treatment protocols in the liquefaction of freshly clotted large-volume human blood samples serving as an *in vitro* hematoma phantom. Specifically, two of the typical BH regimes involving longer (10 ms) and shorter (2 ms) pulses, and a hybrid histotripsy regime using 0.4-ms pulses were used (Eranki et al. 2018) in combination with continuous HIFU focus translation along a square-wave trajectory. The optimal spacing between the meanders and layers was defined based on the geometric parameters of single lesions (for BH regimes) and the width of lesion lines (for a hybrid regime) induced by each pulsing protocol.

All three regimes successfully generated fluid-filled voids in gelatinous hematoma phantoms within clinically relevant times (3−4 mL within 2−11 min). The hybrid histotripsy regime achieved the most uniformly shaped void, based on the absence of discrete clot filaments or lesion "tails" seen in B-mode images of the lesions, and the highest liquefaction rate of 2.62 mL/min. This thrombolysis rate was comparable to the clinical rates of thermal HIFU ablation of soft tissue (Illing et al. 2005; Ikink et al 2015) and was more than five times higher than that achieved previously in bovine blood clots for combined CH and BH raster treatment at a 1.5-MHz frequency (Khokhlova et al., 2016b). In the same study, a slightly higher thrombolysis rate of 2.8 mL/min was achieved using a 1-MHz transducer, which required higher acoustic power. The inverse dependence of the liquefied lesion size on frequency is well documented for both BH (Khokhlova et al. 2011) and other histotripsy methods such as microtripsy (Lin et al. 2014a). For example, a thrombolysis rate of 16.6 mL/min (Gerhardson et al. 2017) was achieved with transcranial microtripsy at a frequency of 250 kHz. However, to facilitate the efficient low-frequency microtripsy approach, a highly focused hemispherical HIFU transducer was required in that study, which is not feasible for the majority of intra-abdominal and retroperitoneal hematomas.

Continuous translation of the transducer focus within targeted region was performed in this study by mechanical manipulation of the sample with a 3-D positioning system. Therefore some time was spent on switching the focus position between the adjacent meanders and layers. These stops were not included in the treatment time calculation as they could be avoided by the use of electronic steering of the focus or the use of a more advanced positioning system (*e.g.,* a robotic arm).

In an additional set of studies, the ability of a less focused 1.5-MHz source ($F\#$ = 1) to liquefy hematoma phantoms with the hybrid histotripsy regime was also examined but proved impossible, likely because of insufficient shock amplitude and, thus, the heating rate at the focus, even at the highest power achievable. Recent experimental studies using human blood clot phantoms Khokhlova et al. 2016b, 2018b; Rosnitskiy et al. 2017) and estimations based on the eqns (1) and ((2) revealed that initiation of boiling within 1 ms at a working frequency of 1.5 MHz requires *in situ* shock amplitudes

higher than 130 MPa and, therefore, cannot be produced by transducers with an $F\# \geq 1$ as the corresponding focal shock amplitudes saturate at a lower value. A higher HIFU frequency could reduce the shock front amplitude required for the hybrid histotripsy regime; for example, an HIFU transducer with an $F\#$ of 1 would enable initiation of boiling within 1 ms at frequencies ≥ 4 MHz, A_s being <90 MPa. However, higher frequencies would result in smaller single lesion volume and reduce the thrombolysis rate (Khokhlova et al. 2011).

One limitation of this study is the difference between the envisioned clinical implementation of the method and its laboratory implementation. First, in a clinical setting, the HIFU beam will be attenuated and aberrated by the overlying inhomogeneous tissues and potentially by the inhomogeneities in the structure of the hematoma itself. The aberration will distort the HIFU beam, shift the focus and may prevent shock formation at the intended point. These effects have to be mitigated using the emerging methods of aberration correction based on pre-operational computed tomography scans or backscattering of nonlinear pulses (Suomi et al. 2018; Martin et al. 2020; Thomas et al. 2021). The overlying tissues may also influence the quality of B-mode imaging guiding the liquefaction process, as reported previously for BH ablation of other abdominal targets (Khokhlova et al., 2019). Further, in a clinical setting, the spatial translation of the HIFU focus would have to be realized either by mechanical translation of the transducer or by electronic steering of the focus.

After the treatment, fine-needle aspirations of the lysates were taken from 6 of 21 samples (2 samples per regime) for subsequent cytological analysis and scanning electron microscopy. Complete destruction of blood cells was observed in all samples, and there was no apparent dependence of debris structure on pulsing protocol. Preliminary studies revealed that fine-needle aspiration has no visually detectable effect on the clot ultrastructure, suggesting that it adequately represented the contents of the obtained lesion.

SEM images of the control untreated samples revealed clot ultrastructure similar to those of control samples reported in the literature (Janis et al. 2002; Sutton et al. 2013; Bester et al. 2018). The liquefied lysate appeared as multiple fused layers of destroyed fibrin fragments covered with cell remnants, making it impossible to define the sizes of individual lysate fragments. Optimal separation of the debris before SEM analysis was achieved by diluting the lesion content with distilled water to a final concentration of 1:50. This simple method allowed for manual sizing of the larger residual fragments, although it led to bursting of the blood cells. The choice of distilled water over isotonic PBS was made in an effort to avoid aggregation of the debris to salt crystals. The fibrin network debris was found to preserve the same ultrastructure in distilled water as in PBS. The predominant part of the fragments was smaller than 20 μm, which corresponded to the results presented in the literature (Khokhlova et al. 2016a; Li et al. 2020). Sizing of the larger debris (>20 μm) revealed that the largest fibrin fragments observed were 150 μm in length, which, under clinical conditions, would most definitely not hinder a fine-needle aspiration with commonly used needles up to 23G (opening of 160 μm and larger).

These results indicate the potential of using histotripsy with continuous focus translation to rapidly and non-invasively break down large hematomas, within a clinically relevant time, into debris sufficiently small for subsequent fine-needle aspiration. The hybrid sub-millisecond histotripsy method resulted in a faster liquefaction rate compared with BH regimes.

CONCLUSIONS

This work aimed to investigate the liquefaction of large human hematomas by continuous delivery of histotripsy pulses of varying length with continuous HIFU focus translation and to refine SEM methods to evaluate the exposure outcomes. Three types of histotripsy approaches (BH with 10- and 2-ms pulses and a hybrid sub-millisecond regime) were used for treating large human hematomas *in vitro*. All regimens yielded volumetric lesions within a clinically relevant time, with the highest thrombolysis rate and the most spatially uniform void achieved with the hybrid pulsing protocol. SEM and cytological analysis of the lysate confirmed complete cell disintegration for all the regimes. Dilution of the lysate in distilled water allowed for manual sizing of the individual debris; most of them were smaller than 20 μm and the largest was 150 μm in length and, thus, unlikely to hinder fine-needle aspiration.

Acknowledgments—This work was supported in part by National Institutes of Health (NIH) Grants R01GM122859 and R01EB007643, RFBR Grant 20-02-00210, the FUSF Global Internship program and student stipends from the "BASIS" Foundation and Vladimir Potanin Fellowship Program. The authors thank Adam Maxwell for his help with the use of a high-power amplifier, Petr Yuldashev for advice in simulations, volunteers at the Dmitry Rogachev National Research Center for their help with donor blood samples and Anatoly Bogdanov from the Electron Microscopy Laboratory of the Biological Faculty of Moscow State University for help with SEM analysis.

Conflict of interest disclosure—The authors declare no conflicts of interest.

REFERENCES

Angster KH, Da Costa V. Chronic hematoma of the neck. Pediatr Emerg Care 2018;34:35–38.

Bawiec CR, Khokhlova TD, Sapozhnikov OA, Rosnitskiy PB, Cunitz BW, Ghanem MA, Hunter C, Kreider W, Schade GR, Yuldashev PV, Khokhlova VA. A prototype therapy system for boiling

histotripsy in abdominal targets based on a 256-element spiral array. IEEE Trans Ultrason Ferroelectr Freq Control 2021;68:1496–1510.
Bernal M, Gennisson JL, Flaud P, Tanter M. Shear wave elastography quantification of blood elasticity during clotting. Ultrasound Med Biol 2012;38:2218–2228.
Bessonova OV, Khokhlova VA, Canney MS, Bailey MR, Crum LA. A derating method for therapeutic applications of high intensity focused ultrasound. Acoust Phys 2010;56:354–363.
Bester J, Matshailwe C, Pretorius E. Simultaneous presence of hypercoagulation and increased clot lysis time due to IL-1β, IL-6 and IL-8. Cytokine 2018;110:237–242.
Bovonratwet P, Fu MC, Tyagi V, Bohl DD, Ondeck NT, Albert TJ, Grauer JN. Incidence, risk factors, and clinical implications of postoperative hematoma requiring reoperation following anterior cervical discectomy and fusion. Spine (Phila Pa 1976) 2019;44:543–549.
Broderick JP, Brott TG, Duldner JE, Tomsick T, Huster G. Volume of intracerebral hemorrhage: A powerful and easy-to-use predictor of 30-day mortality. Stroke 1993;24:987–993.
Buravkov SV, Chernikov VP, Buravkova LB. Simple method of specimen preparation for scanning electron microscopy. Bull Exp Biol Med 2011;151:378–382.
Canney MS, Khokhlova VA, Bessonova OV, Bailey MR, Crum LA. Shock-induced heating and millisecond boiling in gels and tissue due to high intensity focused ultrasound. Ultrasound Med Biol 2010;36:250–267.
Chung KT. Intra-abdominal hematoma following enoxaparin injection. Clin Med Insights Case Rep 2016;9:35–38.
Dohan A, Darnige L, Sapoval M, Pellerin O. Spontaneous soft tissue hematomas. Diagn Interv Imaging 2015;96:789–796.
Elhammady MS, Heros RC, Morcos JJ. Surgical management of asymptomatic carotid stenosis. In: Mohr JP, Wolf PA, Grotta JC, Moskowitz MA, Mayberg M, von Kummer R, (eds). Stroke: Pathophysiology, diagnosis, and management. 5th editionPhiladelphia: Saunders; 2011. p. 1403–1416.
Eranki A, Farr N, Partanen A, Sharma KV, Rossi CT, Rosenberg AZ, Kim A, Oetgen M, Celik H, Woods D, Yarmolenko PS, Kim PCW, Wood BJ. Mechanical fractionation of tissues using microsecond-long HIFU pulses on a clinical MR-HIFU system. Int J Hyperthermia 2018;34:1213–1224.
Garner MR, Taylor SA, Gausden E, Lyden JP. Compartment syndrome: Diagnosis, management, and unique concerns in the twenty-first century. HSS J 2014;10:143–152.
Gerhardson T, Sukovich JR, Pandey AS, Hall TL, Cain CA, Xu Z. Effect of frequency and focal spacing on transcranial histotripsy clot liquefaction, using electronic focal steering. Ultrasound Med Biol 2017;43:2302–2317.
Gersh KC, Nagaswami C, Weisel JW. Fibrin network structure and clot mechanical properties are altered by incorporation of erythrocytes. Thromb Haemost 2009;102:1169–1175.
Hamilton M, Blackstock D. Nonlinear acoustics. San Diego: Academic Press; 1998.
Ikink ME, van Breugel JM, Schubert G, Nijenhuis RJ, Bartels LW, Moonen CT, van den Bosch MA. Volumetric MR-guided high-intensity focused ultrasound with direct skin cooling for the treatment of symptomatic uterine fibroids: Proof-of-concept study. Biomed Res Int 2015;2015 684250.
Illing RO, Kennedy JE, Wu F, ter Haar GR, Protheroe AS, Friend PJ, Gleeson FV, Cranston DW, Phillips RR, Middleton MR. The safety and feasibility of extracorporeal high-intensity focused ultrasound (HIFU) for the treatment of liver and kidney tumours in a Western population. Br J Cancer 2005;93:890–895.
Janis AD, Buckley LA, Nyara AN, Prahl SA, Gregory K. A reconstituted in vitro clot model for evaluating laser thrombolysis. J Thromb Thrombolysis 2002;13:167–175.
Khokhlova TD, Canney MS, Khokhlova VA, Sapozhnikov OA, Crum LA, Bailey MR. Controlled tissue emulsification produced by high intensity focused ultrasound shock waves and millisecond boiling. J Acoust Soc Am 2011;130:3498–3510.
Khokhlova VA, Fowlkes JB, Roberts WW, Schade GR, Xu Z, Khokhlova TD, Hall TL, Maxwell AD, Wang YN, Cain CA. Histotripsy methods in mechanical disintegration of tissue: Towards clinical applications. Int J Hyperthermia 2015;31:145–162.
Khokhlova VA, Yuldashev PV, Rosnitskiy PB, Maxwell AD, Kreider W, Bailey MR, Sapozhnikov OA. Design of HIFU transducers to generate specific nonlinear ultrasound fields. Phys Procedia 2016a;87:132–138.
Khokhlova TD, Monsky WL, Haider YA, Maxwell AD, Wang YN, Matula TJ. Histotripsy liquefaction of large hematomas. Ultrasound Med Biol 2016b;42:1491–1498.
Khokhlova TD, Haider YA, Maxwell AD, Kreider W, Bailey MR, Khokhlova VA. Dependence of boiling histotripsy treatment efficiency on HIFU frequency and focal pressure levels. Ultrasound Med Biol 2017;43:1975–1985.
Khokhlova T, Kuzcevic J, Hunter C, Maxwell A, Khokhlova V, Matula T, Monsky W. Boiling histotripsy liquefaction of large extravascular hematomas: In vitro optimization and device design considerations. Abstract Book of the 6th International Symposium on Focused Ultrasound. 151–152.
Khokhlova T, Rosnitskiy P, Hunter C, Maxwell A, Kreider W, Ter Haar G, Costa M, Sapozhnikov O, Khokhlova V. Dependence of inertial cavitation induced by high intensity focused ultrasound on transducer F-number and nonlinear waveform distortion. J Acoust Soc Am 2018b;144:1160.
Khokhlova TD, Schade GR, Wang YN, Buravkov SV, Chernikov VP, Simon JC, Starr F, Maxwell AD, Bailey MR, Kreider W, Khokhlova VA. Pilot *in vivo* studies on transcutaneous boiling histotripsy in porcine liver and kidney. Sci Rep 2019;9 20176.
Khokhlova VA, Yuldashev PV, Mezdrokhin I, Rosnitskiy P, Karzova MM, Kreider W, Sapozhnikov O. Development of a freely available simulator with graphical interface for modeling nonlinear focused ultrasound fields with shocks. J Acoust Soc Am 2018c;144 (3, Pt 2):1699.
Khokhlova TD, Kucewicz JC, Ponomarchuk EM, Hunter C, Bruce M, Khokhlova VA, Matula TJ, Monsky W. Effect of stiffness of large extravascular hematomas on their susceptibility to boiling histotripsy liquefaction in vitro. Ultrasound Med Biol 2020;46:2007–2016.
Li Y, Liu Y, Li R, Lu M, Wang X, Geng Y, Zhang Q, Wan M. Histotripsy liquefaction of large hematoma for intracerebral hemorrhage using millisecond-length ultrasound pulse groups combined with fundamental and second harmonic superposition: A preliminary study. Ultrasound Med Biol 2020;46:1244–1257.
Lin KW, Duryea AP, Kim Y, Hall TL, Xu Z, Cain CA. Dual-beam histotripsy: a low-frequency pump enabling a high-frequency probe for precise lesion formation. IEEE Trans Ultrason Ferroelectr Freq Control 2014a;61:325–340.
Lin KW, Kim Y, Maxwell AD, Wang TY, Hall TL, Xu Z, Fowlkes JB, Cain CA. Histotripsy beyond the intrinsic cavitation threshold using very short ultrasound pulses: Microtripsy. IEEE Trans Ultrason Ferroelectr Freq Control 2014b;61:251–265.
Martin E, Jaros J, Treeby BE. Experimental validation of k-wave: Nonlinear wave propagation in layered, absorbing fluid media. IEEE Trans Ultrason Ferroelectr Freq Control 2020;67:81–91.
Maxwell AD, Cain CA, Hall TL, Fowlkes JB, Xu Z. Probability of cavitation for single ultrasound pulses applied to tissues and tissue-mimicking materials. Ultrasound Med Biol 2013;39:449–465.
Maxwell AD, Yuldashev PV, Kreider W, Khokhlova TD, Schade GR, Hall TL, Sapozhnikov OA, Bailey MR, Khokhlova VA. A prototype therapy system for transcutaneous application of boiling histotripsy. IEEE Trans Ultrason Ferroelectr Freq Control 2017;64:1542–1557.
Nahirnyak VM, Yoon SW, Holland CK. Acousto-mechanical and thermal properties of clotted blood. J Acoust Soc Am 2006;119:3766–3772.
Pahk KJ, de Andrade MO, Gélat P, Kim H, Saffari N. Mechanical damage induced by the appearance of rectified bubble growth in a viscoelastic medium during boiling histotripsy exposure. Ultrason Sonochem 2019;53:164–177.
Pahk KJ, Lee S, Gélat P, de Andrade MO, Saffari N. The interaction of shockwaves with a vapour bubble in boiling histotripsy: The shock scattering effect. Ultrason Sonochem 2021;70 105312.
Parsons JE, Cain CA, Abrams GD, Fowlkes JB. Pulsed cavitational ultrasound therapy for controlled tissue homogenization. Ultrasound Med Biol 2006;32:115–129.

Ponomarchuk EM, Buravkov SV, Rosnitskiy PB, Tsysar SA, Karzova MM, Kunturova AV, Topchu KD, Sapozhnikov OA, Khokhlova VA. Cytological and ultrastructural analysis of mechanically liquefied lesions generated using boiling histotripsy in a porcine model of hematoma ex vivo. Abstract book of the 19th International Symposium of ISTU/5th European Symposium of EUFUS. : ISTU/EUFUS; 2019. p. 51.

Pretorius E, Oberholzer HM, van der Spuy WJ, Franz RC. Comparing techniques: The use of recalcified plasma in comparison with citrated plasma alone and in combination with thrombin in ultrastructural studies. Hematology 2011;16:337–340.

Rosnitskiy PB, Yuldashev PV, Sapozhnikov OA, Maxwell AD, Kreider W, Bailey MR, Khokhlova VA. Design of HIFU transducers for generating specified nonlinear ultrasound fields. IEEE Trans Ultrason Ferroelectr Freq Control 2017;64:374–390.

Shung KK, Fei DY, Yuan YW, Reeves WC. Ultrasonic characterization of blood during coagulation. J Clin Ultrasound 1984;12:147–153.

Simon JC, Sapozhnikov OA, Khokhlova VA, Wang YN, Crum LA, Bailey MR. Ultrasonic atomization of tissue and its role in tissue fractionation by high intensity focused ultrasound. Phys Med Biol 2012;57:8061–8078.

Smith TO, Hunt NJ, Wood SJ. The physiotherapy management of muscle haematomas. Phys Ther Sport 2006;7:201–209.

Suomi V, Jaros J, Treeby B, Cleveland RO. Full modeling of high-intensity focused ultrasound and thermal heating in the kidney using realistic patient models. IEEE Trans Biomed Eng 2018;65:2660–2670.‘

Sutton JT, Ivancevich NM, Perrin SR, Jr, Vela DC, Holland CK. Clot retraction affects the extent of ultrasound-enhanced thrombolysis in an ex vivo porcine thrombosis model. Ultrasound Med Biol 2013;39:813–824.

Thomas GPL, Khokhlova TD, Bawiec CR, et al. Phase-aberration correction for HIFU therapy using a multielement array and backscattering of nonlinear pulses. IEEE Trans Ultrason Ferroelectr Freq Control 2021;68:1040–1050.

Vlaisavljevich E, Xu Z, Maxwell A, Mancia L, Zhang X, Lin KW, Duryea A, Sukovich J, Hall T, Johnsen E, Cain C. Effects of temperature on the histotripsy intrinsic threshold for cavitation. IEEE Trans Ultrason Ferroelectr Freq Control 2016;63:1064–1077.

Weisel JW, Litvinov RI. The biochemical and physical process of fibrinolysis and effects of clot structure and stability on the lysis rate. Cardiovasc Hematol Agents Med Chem 2008;6:161–180.

Weiss S, Messner F, Huth M, Weissenbacher A, Denecke C, Aigner F, Brandl A, Dziodzio T, Sucher R, Boesmueller C, Oellinger R, Schneeberger S, Oefner D, Pratschke J, Biebl M. Impact of abdominal drainage systems on postoperative complication rates following liver transplantation. Eur J Med Res 2015;20:66.

Wicks JD, Silver TM, Bree RL. Gray scale features of hematomas: An ultrasonic spectrum. AJR Am J Roentgenol 1978;131:977–980.

Yuldashev PV, Mezdrokhin IS, Khokhlova VA. Wide-angle parabolic approximation for modeling high-intensity fields from strongly focused ultrasound transducers. Acoust Phys 2018;64:309–319.

Zhang X, Owens GE, Cain CA, Gurm HS, Macoskey J, Xu Z. Histotripsy thrombolysis on retracted clots. Ultrasound Med Biol 2016;42:1903–1918.